



OPEN

Bio-inspired mineralization of nanostructured TiO₂ on PET and FTO films with high surface area and high photocatalytic activity

Yoshitake Masuda

Nanostructured TiO₂ coatings were successfully formed on polyethylene terephthalate (PET) films and fluorine-doped tin oxide (FTO) films in aqueous solutions. They contained an assembly of nanoneedles that grow perpendicular to the films. The surface area of the coatings on PET films reached around 284 times that of a bare PET film. Micro-, nano-, or subnanosized surface roughness and inside pores contributed to the high nitrogen adsorption. The coatings on FTO films showed an acetaldehyde removal rate of 2.80 μmol/h; this value is similar to those of commercial products certified by the Photocatalysis Industry Association of Japan. The rate increased greatly to 10.16 μmol/h upon annealing in air at 500 °C for 4 h; this value exceeded those of commercial products. Further, the coatings showed a NO_x removal rate of 1.04 μmol/h; this value is similar to those of commercial products. The rate decreased to 0.42 μmol/h upon annealing. NO_x removal was affected by the photocatalyst's surface area rather than its crystallinity.

Metal oxides are useful for industrial applications such as gas sensors, batteries, and artificial photosynthesis^{1–12}. For example, SnO₂ micropatterns were fabricated on a polymer film¹ and a silicon substrate² using a patterned octadecyltrimethoxysilane self-assembled monolayer template. The sensitivity of a hydrogen gas sensor with an SnO₂ micropattern increased linearly with increasing SnO₂ crystallinity. SnO₂ could also be used to fabricate a lightweight flexible gas sensor on a polymer film. A porous iron vanadate (FeVO₄) thick film consisting of disordered nanorods was fabricated by a hydrothermal method for gas penetration and permeation¹². The probed I–V behavior and ultraviolet–visible spectroscopy measurements confirmed the semiconducting nature of triclinic FeVO₄ (E_g = 2.72 eV) and revealed that the activation energy for electric conduction was 0.46 eV. The best gas sensitivity of 0.29 ± 0.01 (m = –3.4 ± 0.1) was obtained at optimal working temperature of 250 °C. SnO₂ nanowires were fabricated for an H₂S gas sensor³. They were functionalized with copper particles during chemical vapor deposition. A CuO@SnO₂ p–n heterojunction was fabricated by oxidizing Cu to CuO. The fabricated sensor demonstrated high sensitivity and selectivity for H₂S gas. VO₂ nanobelts or nanoparticles were fabricated by a hydrothermal method for thermochromic devices⁴. Nanoparticles showed high phase transition enthalpy (ΔH = 32.4 J/g) and VO₂-PET composite films showed optical switching characteristics (T_{lum} = 33.5%, ΔT_{sol} = 16.0%). A dye-sensitized solar cell was prepared with a ZnO@TiO₂ core shell nanorod array via a low-temperature solution method⁵. High-aspect-ratio ZnO nanorod arrays were covered with a TiO₂ shell. The TiO₂ shell increased the short circuit current (from 4.2 to 5.2 mA/cm²), open circuit voltage (from 0.6 to 0.8 V), fill factor (from 42.8 to 73.02%), and overall cell efficiency (from 1.1 to 3.03%). ZnO nanorods were grown on a highly conductive sandwich-like seed layer (ZnO seed layer/Ag nanowires/ZnO seed layer) and modified with α-Fe₂O₃ nanoparticles⁶. ZnO nanorods showed high potential for Ca²⁺ sensing in water or serum samples. They can be applied to drinking and irrigation water as well as to clinical analysis. A sensitive and selective sunlight-driven photoelectrochemical sensor was developed for the direct detection and reduction of chromium(VI)¹¹. It was based on single-crystal rutile TiO₂ nanorods decorated with gold nanoparticles. It showed high sensitivity under

National Institute of Advanced Industrial Science and Technology (AIST), 2266-98 Anagahora, Shimoshidami, Morioka-ku, Nagoya 463-8560, Japan. email: masuda-y@aist.go.jp

solar simulator illumination. Evaluations of real water samples showed excellent anti-interference and recovery capabilities. Metal oxide nanomaterials and a biosensor fabricated using them were reviewed⁷. Nanomaterial deposition on conductive electrodes is a crucial step for achieving high performance, and a simple, stable, and reproducible method is considered essential for depositing nanomaterials for fabricating a biosensor.

Many devices have reaction sites on the metal oxide surface, and therefore, they need to have a large surface area. In addition, studies are developing new devices by using the characteristic surface structure of metal oxides. Controlling the size, shape, and crystallinity of the metal oxide is known to greatly affect the device characteristics, and new metal oxide materials are being actively developed. There is also a strong need to control the shape and even the exposed crystal plane after the metal oxide material is crystallized. Especially, nanostructured TiO₂ films with high surface area and high photocatalytic activity are strongly required for photocatalysts and related devices. Performance of the nanostructured TiO₂ films is strongly affected by the size, shape, crystallinity, and the exposed crystal plane. The development of high performance nanostructured TiO₂ films is a powerful demonstration of precise control of the size, shape, crystallinity, and the exposed crystal plane.

Metal oxide nano-/microstructures have also been synthesized in animals and plants. The size, shape, crystallinity, and surface structure of metal oxides in aqueous solutions were controlled at room temperature and atmospheric pressure. They are called “Bio-mineralization” and have created a new academic field, “Bio-inspired mineralization”. In the bio-inspired mineralization, we learn from nature and aim to develop novel materials that are not in nature.

This study investigates the bio-inspired mineralization of nanostructured TiO₂. Nanostructured TiO₂ was formed on polymer or inorganic films in aqueous solutions. Further, its surface area and photocatalytic properties were investigated.

Experimental

Ammonium hexafluorotitanate ([NH₄]₂TiF₆) (Morita Chemical Industries Co., Ltd., FW: 15, purity 96.0%) and boric acid (H₃BO₃) (Kishida Chemical Co., Ltd., FW: 61, purity 99.5%) were used as received. Nanostructured TiO₂ films were crystallized on polyethylene terephthalate (PET) films or fluorine-doped tin oxide (FTO) films in an aqueous solution containing ammonium hexafluorotitanate (50 mM) and boric acid (150 mM) at 50 °C for 24 h.

The morphology of the nanostructured TiO₂ film on the PET film was observed using a field-emission scanning electron microscope (FE-SEM; JSM-6335F, JEOL Ltd.) at 20 kV. Nitrogen adsorption–desorption isotherms were obtained using Autosorb-1 (Quantachrome Instruments). Nanostructured TiO₂ films on PET films were outgassed at 110 °C under 10⁻² mmHg for more than 6 h prior to measurement. The specific surface area was calculated by the Brunauer–Emmett–Teller (BET) method using adsorption isotherms. The pore size distribution was calculated by the Barrett–Joyner–Halenda (BJH) method using desorption isotherms. The photocatalytic properties of the nanostructured TiO₂ on FTO films were evaluated at the Kanagawa Academy of Science and Technology (KAST), Japan, based on Japanese Industrial Standards (JIS).

Results and discussion

Bio-inspired mineralization of nanostructured TiO₂. Ten sheets of PET films (50 mm long × 50 mm wide × 0.1 mm thick) were pasted on glass plates with polytetrafluoroethylene tapes. Ammonium hexafluorotitanate (10.31 g) and boric acid (9.321 g) were dissolved in 1,000 mL of distilled hot water¹³. The concentrations of ammonium hexafluorotitanate and boric acid were 50 and 150 mM, respectively. PET films were exposed to vacuum-ultraviolet light for 20 min in air using a low-pressure mercury lamp (PL16-110, SEN Lights Co.). They were immersed in the solutions at 50 °C for 24 h. The titanium oxide-formed surface of the PET films faced obliquely downward. Therefore, even if homogeneously nucleated titanium oxide particles formed in the solution settle, they are less likely to be deposited on the PET film. Further, the PET film is less likely to be bent or deformed in the solution because it is attached to the glass plate. Moreover, titanium oxide is formed only on the PET film surface because the back surface of the film is in close contact with the glass plate. Thereafter, the glass plates were removed from the solution. The PET films were peeled off from the glass plates, washed with running water, and dried under a strong air flow.

Nanostructured TiO₂ with high surface area. PET films were uniformly covered with nanostructured TiO₂ (Fig. 1a). The coatings had an uneven surface structure (Fig. 1b). The needle-like surface structures had size of ~5–10 nm (Fig. 1c). Each needle had nanosized surface asperities.

The mass of the PET film was measured before and after immersion in the aqueous solution. The mass of nanostructured TiO₂ was calculated from the difference in mass before and after immersion. The composite was cut to obtain rectangular pieces with dimensions of ~3 mm × 10 mm. All of these pieces were filled in a glass sample holder for gas adsorption measurements. The gas adsorption amount of the composite can be measured with almost no influence of the PET film, and the measured gas adsorption amount of the composite can be regarded as the gas adsorption amount of nanostructured TiO₂.

Nanostructured TiO₂ showed nitrogen adsorption–desorption isotherms (Fig. 2a). The pore size distribution of nanostructured TiO₂ was calculated from the nitrogen desorption isotherm by the BJH method (Fig. 2b). Nanostructured TiO₂ had inside pores and/or interparticle spaces of ~2–100 nm. The result did not indicate whether nanostructured TiO₂ has pores of 1 nm or less because such pores cannot be estimated by the BJH method. The BET specific surface area was calculated to be 503.6 m²/g (Fig. 2c). The total surface area of nanostructured TiO₂ was calculated by multiplying this value by the mass of nanostructured TiO₂. The ratio of the surface area to the substrate projected area was calculated to around 284 times that of a bare PET film by dividing the total surface area of nanostructured TiO₂ by the projected area of substrates (25,000 mm², 50 mm × 50 mm × 10

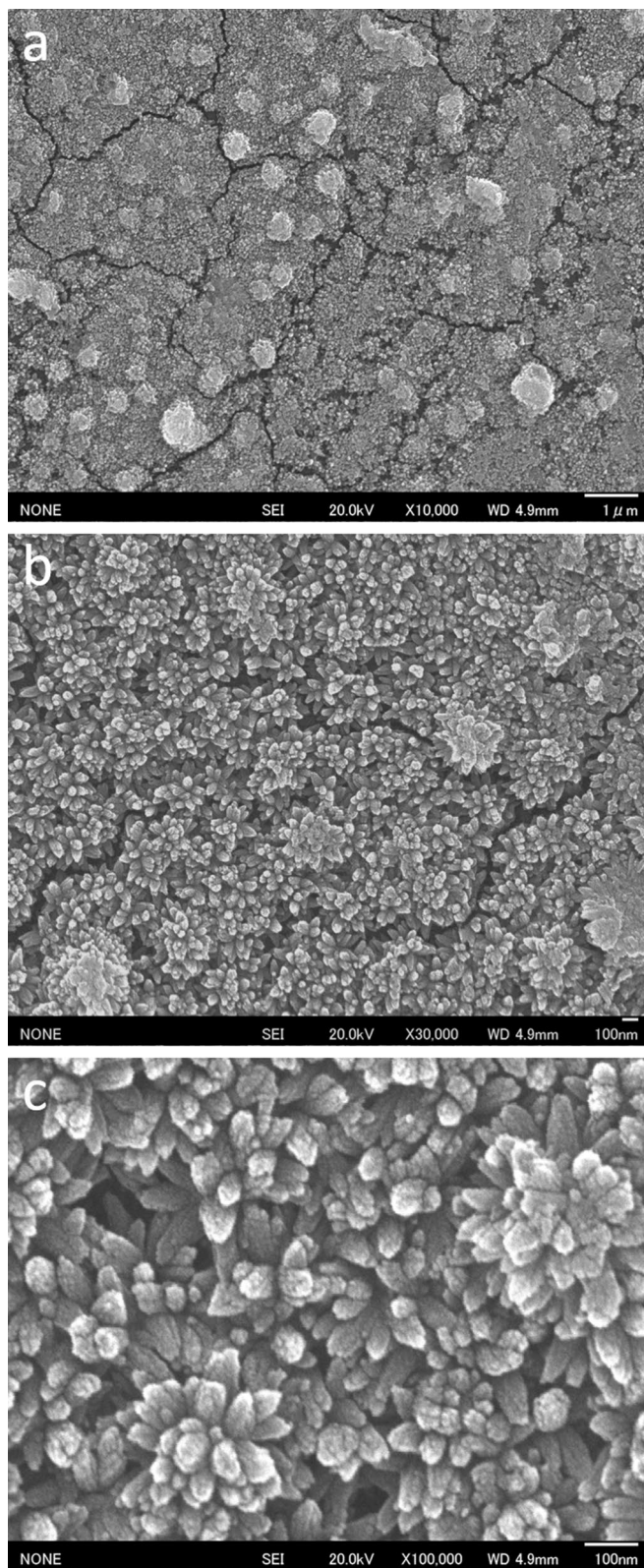


Figure 1. (a) FE-SEM micrograph of nanostructured TiO₂ on a PET film. The nanostructured TiO₂ was formed in an aqueous solution using liquid-phase crystal growth. (b), (c) Magnified FE-SEM micrographs of (a).

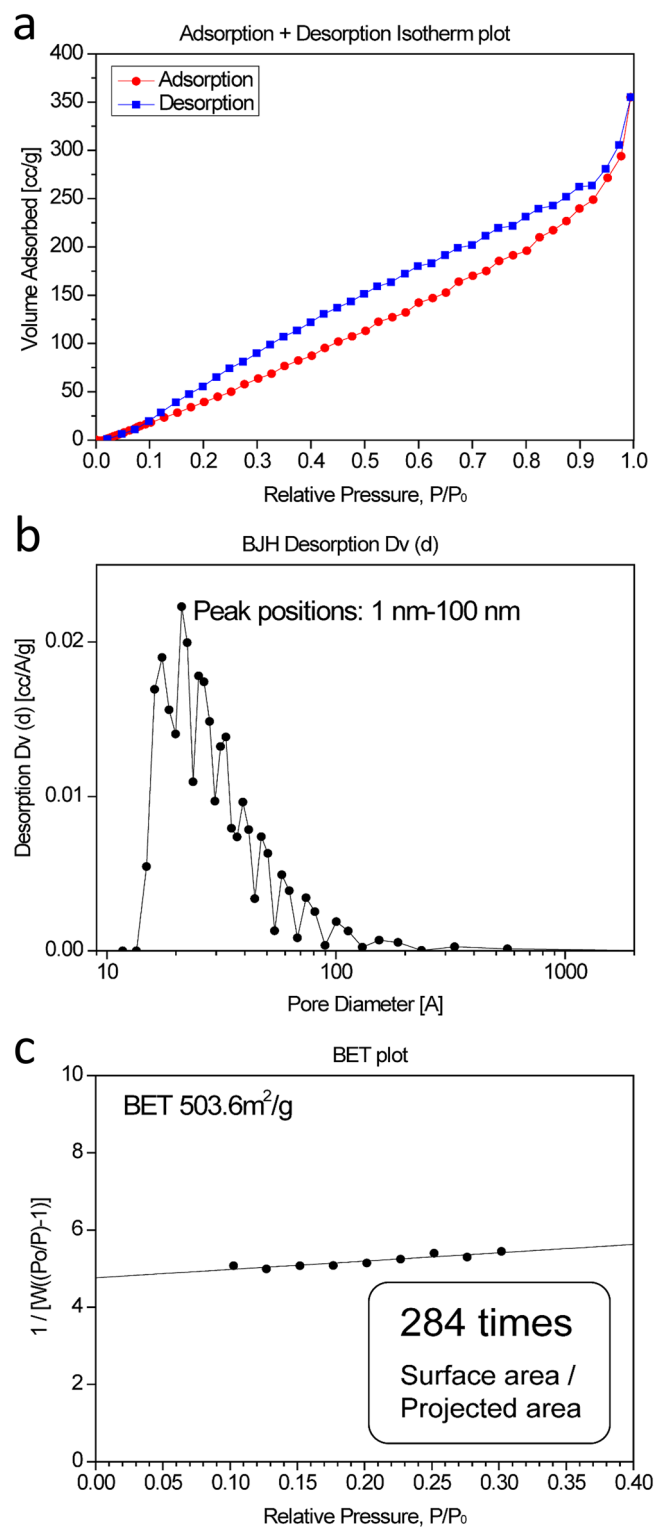


Figure 2. (a) N_2 adsorption–desorption isotherm of nanostructured TiO_2 on a PET film. (b) Pore size distribution calculated from N_2 adsorption data of nanostructured TiO_2 on a PET film using BJH equation. (c) BET surface area of nanostructured TiO_2 on a PET film. Inset: ratio of surface area to substrate projected area.

sheets). The total surface area is not affected by the error of the weight of the nanostructured TiO_2 in this calculation method, and therefore, it can be determined accurately. To the best of the authors' knowledge, the TiO_2 film surface area was the highest ever reported. Nanostructured TiO_2 in this study was considered to be different

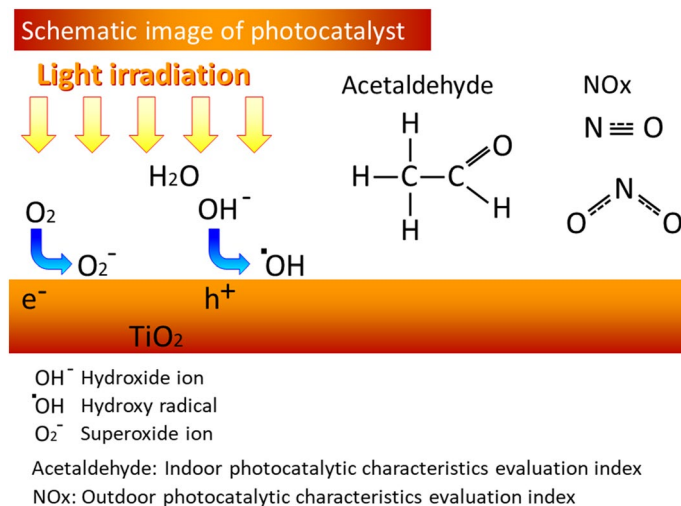


Figure 3. Schematic image of photocatalytic activity.

	Acetaldehyde decomposition characteristics				NO _x decomposition characteristics								
	QA/ $\mu\text{mol/h}$	QC/ $\mu\text{mol/h}$	RA/%	RC/%	QNO _x	Qads	QNO	QNO ₂	Qdes	η_w	Qw1	Qw2	QNo _x
TiO ₂	2.80	4.56	20.6	16.8	1.04	0.08	3.0	1.24	0.8	1,400	12.5	2.42	1.04
TiO ₂ (after annealing at 550 °C for 4 h)	10.16	16.84	74.8	60.2	0.42	0.08	2.7	1.68	0.7	2,100	7.34	1.28	0.42

Table 1. Photocatalytic properties of nanostructured TiO₂. They were evaluated based on JIS R 1701-2: 2008 (left, acetaldehyde removal performance) and JIS R 1701-1: 2010 (right, NO_x removal performance).

from general nanostructured TiO₂ reported elsewhere. Micro-, nano-, and subnanosized surface roughness and inside pores contributed to increased nitrogen adsorption. Surface crystal defects such as kinks, terraces, and secondary nuclei were also considered to contribute to increased nitrogen adsorption.

Nanostructured TiO₂ with high photocatalytic activity. FTO films were exposed to vacuum-ultraviolet light for 20 min. They were immersed in the solutions containing ammonium hexafluorotitanate (50 mM) and boric acid (150 mM) at 50 °C for 24 h. The photocatalytic properties of the nanostructured TiO₂ on FTO films were evaluated based on JIS R 1701-2: 2008 (acetaldehyde removal performance) and JIS R 1701-1: 2010 (nitrogen oxide (NO_x) removal performance). Acetaldehyde and NO_x serve as evaluation indices for indoor and outdoor photocatalytic activity, respectively. Materials with high photocatalytic activity for acetaldehyde and NO_x can be used in building interiors and exteriors, respectively. The photocatalytic characteristics were evaluated using two FTO films (50 mm × 26 mm × 1.1 mm in thickness) (AGC Fabritech Co., Ltd., TOC substrate (DU film)). The FTO layer (0.1 mm in thickness) was formed on a glass substrate (0.1 mm in thickness). The size of the test piece was around half of the JIS-specified size (50 mm × 100 mm). The measured values excluding regeneration efficiency for NO_x removal characteristics were thus doubled.

In general, light irradiation on a photocatalytic material such as TiO₂ generates electrons and holes on the surface (Fig. 3). Oxygen and water in the air react with electrons and holes, respectively. These reactions produce hydroxy (OH) radicals and superoxide ions on the titanium dioxide surface. OH radicals have strong oxidizing power and remove electrons from acetaldehyde molecules. Acetaldehyde molecules lose electrons and break bonds. They were converted to CO₂ and/or H₂O that were released to the atmosphere.

Acetaldehyde was removed from the sample at the rate of 2.80 $\mu\text{mol/h}$, and its removal ratio was 20.6% (Table 1). This rate was similar to that of commercial products certified by the Photocatalysis Industry Association of Japan¹⁴ (Fig. 4). Further, acetaldehyde was converted to CO₂ at the rate of 4.56 $\mu\text{mol/h}$, and its conversion ratio was 16.8%.

The amount of NO_x removed was 1.04 μmol (Table 1). This value was similar to that of commercial products (Fig. 5). The NO_x adsorption and desorption amounts were 0.08 and 0.8 μmol , respectively. The amount of nitric oxide removed was 3.0 μmol . The amount of nitrogen dioxide generated was 1.24 μmol .

The regeneration efficiency upon washing with water was 1,400% (no conversion). The first and second elution amounts of NO_x were 12.50 and 2.42 μmol , respectively. The regeneration efficiency exceeded 100%, suggesting that NO_x was generated from the sample during the test and was added to the NO_x elution amount. This result indicated that nanostructured TiO₂ contained nitrogen inside and/or on its surface. Ammonium hexafluorotitanate is one of the sources of nitrogen.

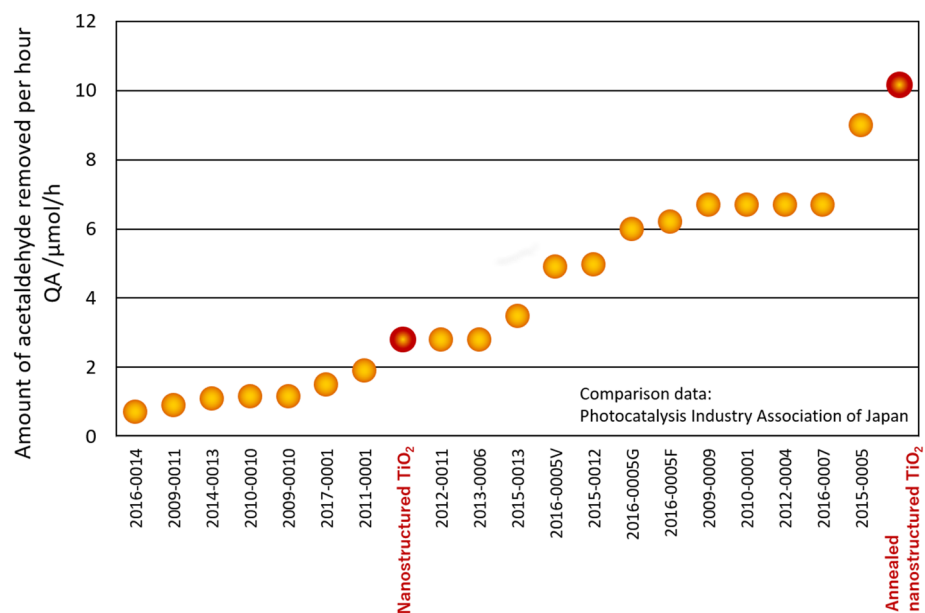


Figure 4. Comparison of acetaldehyde decomposition characteristics with those of commercial products certified by the Photocatalysis Industry Association of Japan.

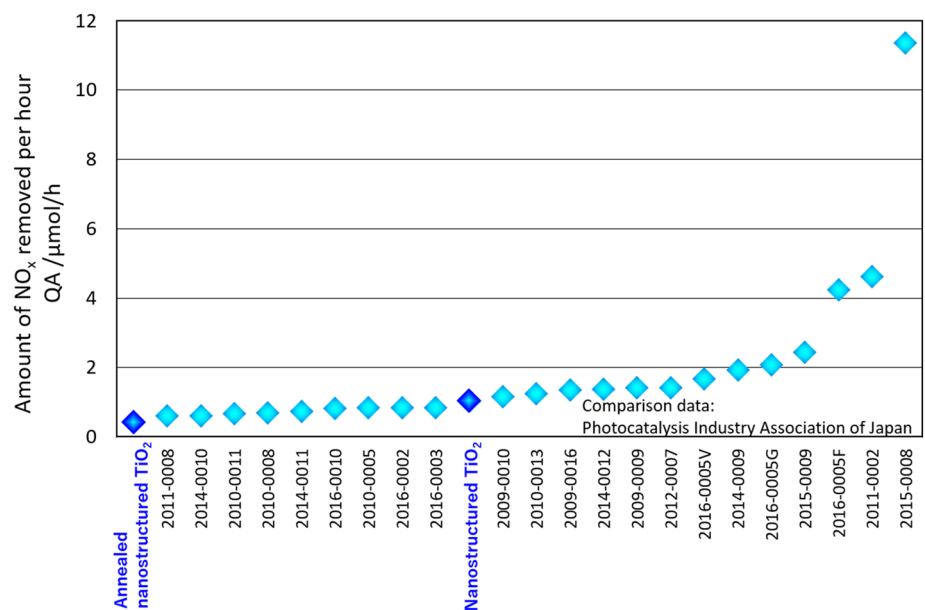


Figure 5. Comparison of NO_x decomposition characteristics with those of commercial products certified by the Photocatalysis Industry Association of Japan.

Annealed nanostructured TiO_2 with high photocatalytic activity. Nanostructured TiO_2 on FTO films were annealed at 500 °C in air for 4 h. In general, high-temperature treatment was considered to improve crystallinity but reduces internal vacancies and surface defects. Photocatalytic properties are affected by both changes.

Notably, the acetaldehyde removal rate increased greatly from 2.80 to 10.16 $\mu\text{mol/h}$ upon annealing, and the removal ratio was 74.8% (Table 1). The rate exceeded that of commercial products (Fig. 4). This was one of the advantages of nanostructured TiO_2 . Further, acetaldehyde was converted to CO_2 at the rate of 16.84 $\mu\text{mol/h}$, and its conversion ratio was 60.2%.

The NO_x removal rate decreased from 1.04 to 0.42 $\mu\text{mol/h}$ upon annealing (Table 1, Fig. 5). NO_x removal was affected by the photocatalyst's surface area rather than its crystallinity. The NO_x adsorption and desorption amounts were 0.08 and 0.7 μmol , respectively. The amount of nitric oxide removed was 2.7 μmol . The amount of

NO_x generated was 1.68 μmol . The regeneration efficiency upon washing with water was 2,100% (no conversion). The first and second elution amounts of NO_x were 7.34 and 1.28 μmol , respectively.

Conclusions

Nanostructured TiO_2 was formed on PET films in aqueous solutions. Nanostructured TiO_2 coatings showed high N_2 adsorption. The BET specific surface area was $\sim 503.6 \text{ m}^2/\text{g}$ and the ratio of the surface area to the substrate projected area reached around 284 times that of a bare PET film. Furthermore, the photocatalytic property of nanostructured TiO_2 on FTO films was evaluated. The acetaldehyde removal rate increased greatly from 2.80 to 10.16 $\mu\text{mol h}$ upon annealing. This value exceeded that of commercial products (Fig. 4). The amount of NO_x removed was 1.04 μmol ; this was similar to that of commercial products. This value decreased to 0.42 $\mu\text{mol/h}$ upon annealing. NO_x removal was affected by the photocatalyst's surface area rather than its crystallinity. The study results revealed that nanostructured TiO_2 had different nanostructure and surface conditions. These contributed to the high surface area and high photocatalytic activity. In particular, the acetaldehyde decomposition characteristics were higher than those of commercial products. Nanostructured TiO_2 can be used for low-cost, large-area coating of various substrates such as polymer films. The high surface area and high photocatalytic activity can be used for various applications to building interior materials.

Received: 19 September 2019; Accepted: 27 July 2020

Published online: 11 August 2020

References

- Shirahata, N. & Hozumi, A. Etchingless microfabrication of a thick metal oxide film on a flexible polymer substrate. *Chem. Mater.* **17**, 20–27. <https://doi.org/10.1021/cm0490165> (2005).
- Shirahata, N. *et al.* Reliable monolayer-template patterning of SnO_2 thin films from aqueous solution and their hydrogen-sensing properties. *Adv. Func. Mater.* **14**, 580–588 (2004).
- Giebelhaus, I. *et al.* One-dimensional CuO-SnO_2 p–n heterojunctions for enhanced detection of H_2S . *J. Mater. Chem. A* **1**, 11261–11268. <https://doi.org/10.1039/C3TA11867C> (2013).
- Dong, B. *et al.* Phase and morphology evolution of VO_2 nanoparticles using a novel hydrothermal system for thermochromic applications: The growth mechanism and effect of ammonium (NH_4^+). *RSC Adv.* **6**, 81559–81568. <https://doi.org/10.1039/C6RA14569H> (2016).
- Goh, G. K. L., Le, H. Q., Huang, T. J. & Hui, B. T. T. Low temperature grown ZnO@TiO_2 core shell nanorod arrays for dye sensitized solar cell application. *J. Solid State Chem.* **214**, 17–23. <https://doi.org/10.1016/j.jssc.2013.11.035> (2014).
- Ahmad, R., Tripathy, N., Ahn, M.-S., Yoo, J.-Y. & Hahn, Y.-B. Preparation of a highly conductive seed layer for calcium sensor fabrication with enhanced sensing performance. *ACS Sens.* **3**, 772–778. <https://doi.org/10.1021/acssensors.7b00900> (2018).
- Ahmad, R. *et al.* Deposition of nanomaterials: A crucial step in biosensor fabrication. *Mater. Today Commun.* **17**, 289–321. <https://doi.org/10.1016/j.mtcomm.2018.09.024> (2018).
- Wang, M. *et al.* Novel synthesis of pure $\text{VO}_2@\text{SiO}_2$ core@shell nanoparticles to improve the optical and anti-oxidant properties of a VO_2 film. *RSC Adv.* **6**, 108286–108289. <https://doi.org/10.1039/C6RA20636K> (2016).
- Liu, P. *et al.* Ultrathin VO_2 nanosheets self-assembled into 3D micro/nano-structured hierarchical porous sponge-like micro-bundles for long-life and high-rate Li-ion batteries. *J. Mater. Chem. A* **5**, 8307–8316. <https://doi.org/10.1039/C7TA00270J> (2017).
- Jalali, M. *et al.* TiO_2 surface nanostructuring for improved dye loading and light scattering in double-layered screen-printed dye-sensitized solar cells. *J. Appl. Electrochem.* **45**, 831–838. <https://doi.org/10.1007/s10800-015-0852-x> (2015).
- Siavash, R. *et al.* AuPd bimetallic nanoparticle decorated TiO_2 rutile nanorod arrays for enhanced photoelectrochemical water splitting. *J. Appl. Electrochem.* **48**, 995–1007. <https://doi.org/10.1007/s10800-018-1231-1> (2018).
- Lehnen, T., Válddor, M., Nižňanský, D. & Mathur, S. Hydrothermally grown porous FeVO_4 nanorods and their integration as active material in gas-sensing devices. *J. Mater. Chem. A* **2**, 1862–1868. <https://doi.org/10.1039/C3TA12821K> (2014).
- Masuda, Y., Ohji, T. & Kato, K. Multineedle TiO_2 nanostructures, self-assembled surface coatings, and their novel properties. *Cryst. Growth Des.* **10**, 913–922. <https://doi.org/10.1021/cg901238m> (2010).
- Photocatalysis Industry Association of Japan, <https://www.piaj.gr.jp/roller/en/>.

Author contributions

Y. M. wrote the main manuscript text, prepared figures, and reviewed the manuscript.

Competing interests

The author declares no competing interests.

Additional information

Correspondence and requests for materials should be addressed to Y.M.

Reprints and permissions information is available at www.nature.com/reprints.

Publisher's note Springer Nature remains neutral with regard to jurisdictional claims in published maps and institutional affiliations.



Open Access This article is licensed under a Creative Commons Attribution 4.0 International License, which permits use, sharing, adaptation, distribution and reproduction in any medium or format, as long as you give appropriate credit to the original author(s) and the source, provide a link to the Creative Commons license, and indicate if changes were made. The images or other third party material in this article are included in the article's Creative Commons license, unless indicated otherwise in a credit line to the material. If material is not included in the article's Creative Commons license and your intended use is not permitted by statutory regulation or exceeds the permitted use, you will need to obtain permission directly from the copyright holder. To view a copy of this license, visit <http://creativecommons.org/licenses/by/4.0/>.

© The Author(s) 2020